Heat-Transport Mechanisms in Superlattices

By *Yee Kan Koh,* Yu Cao, David G. Cahill,* and *Debdeep Jena*

The heat transport mechanisms in superlattices are identified from the cross-plane thermal conductivity Λ of $(AlN)_x$–$(GaN)_y$ superlattices measured by time-domain thermoreflectance. For $(AlN)_{4.1\ nm}$–$(GaN)_{55\ nm}$ superlattices grown under different conditions, Λ varies by a factor of two; this is attributed to differences in the roughness of the AlN/GaN interfaces. Under the growth condition that gives the lowest Λ, Λ of $(AlN)_{4\ nm}$–$(GaN)_y$ superlattices decreases monotonically as y decreases, $\Lambda = 6.35\ W\ m^{-1}\ K^{-1}$ at $y = 2.2$ nm, 35 times smaller than Λ of bulk GaN. For long-period superlattices ($y > 40$ nm), the mean thermal conductance G of AlN/GaN interfaces is independent of y, $G \approx 620\ MW\ m^{-2}\ K^{-1}$. For $y < 40$ nm, the apparent value of G increases with decreasing y, reaching $G \approx 2\ GW\ m^{-2}\ K^{-1}$ at $y < 3$ nm. MeV ion bombardment is used to help determine which phonons are responsible for heat transport in short period superlattices. The thermal conductivity of an $(AlN)_{4.1\ nm}$–$(GaN)_{4.9\ nm}$ superlattice irradiated by 2.3 MeV Ar ions to a dose of 2×10^{14} ions cm^{-2} is reduced by <35%, suggesting that heat transport in these short-period superlattices is dominated by long-wavelength acoustic phonons. Calculations using a Debye-Callaway model and the assumption of a boundary scattering rate that varies with phonon-wavelength successfully capture the temperature, period, and ion-dose dependence of Λ.

1. Introduction

Superlattices are important structures for thermoelectric applications because of their potential for achieving high efficiency for thermoelectric energy conversion.[1,2] Despite numerous theoretical and experimental studies, basic understanding of the thermal conductivity Λ of superlattices is incomplete.[3] In semiconductors, heat is carried by wave-like lattice vibrations, i.e., phonons, with a broad distribution of mean-free-paths ℓ.[4] For long-period semiconductor superlattices (i.e., $\ell < h$, where h is the thickness of the individual layers in the superlattice), Λ is reduced by the finite transmission coefficient of phonons across interfaces;[3,5] this fundamental transport property of the interface is typically referred to as the thermal conductance of the interface.[6] This simple picture cannot, however, explain heat transport in short-period superlattices (i.e., $\ell > h$) because the thermal conductivities of short-period superlattices do not decrease linearly with superlattice period. Even generic understanding of which lattice modes dominate heat transport is lacking. For example, optical phonons which do not contribute significantly to the heat conduction in bulk crystals may be the dominant heat carriers in short-period superlattices through tunneling[7] and mode conversions.[8]

To complicate matters further, coherent reflections of long-wavelength acoustic phonons from multiple interfaces may result in the formation of phonon mini-bands, in which phonons transmit across interfaces with high probability but with reduced group velocity.[9] As a result, theory predicts that Λ of superlattices with atomically smooth and abrupt interfaces should *increase* with decreasing period for superlattices with short periods.[10] Indeed, some researchers reported an *increase* of Λ in short-period superlattices,[11,12] but other researchers working on similar materials reported a *decrease* of Λ.[13,14] This inconsistency suggests that, in addition to temperature and period, other parameters, such as interface roughness[15] and lattice mismatch,[16] might be important.

In this paper, we identify the heat transport mechanisms in superlattices from thermal conductivity Λ measurements of $(AlN)_{4\ nm}$–$(GaN)_y$ superlattices over a wide range of GaN thickness, $2\ nm < y < 1000$ nm, and temperature, $90 < T < 600$ K. We affirm that heat conduction in long-period superlattices is controlled by the thermal conductance of interfaces. To elucidate the dominant heat carriers in short-period superlattices, we created point defects in an $(AlN)_{4.1\ nm}$–$(GaN)_{4.9\ nm}$ superlattice by bombardment with 2.3 MeV Ar^+ ions. As high-frequency acoustic and optical phonons are strongly scattered by point defects,[17] the small reduction in Λ that we observe in these ion-bombarded superlattices implies that heat is transported predominantly by long-wavelength acoustic phonons; these long-wavelength phonons are relatively weakly scattered by the superlattice interfaces.

Our study of the thermal transport physics of superlattices is facilitated by our capability for growing GaN-based superlattices with high structural quality.[18] AlN/GaN interfaces grown by molecular beam epitaxy (MBE) are chemically abrupt at monolayer scale with interface roughness of a few monolayers.[19]

Our results are also technologically important. GaN-based heterojunctions and superlattices are emerging material

[*] Y. K. Koh, Prof. D. G. Cahill
Department of Materials Science and Engineering
University of Illinois at Urbana-Champaign
Urbana, Illinois 61801 (USA)
E-mail: ykoh@mrl.uiuc.edu
Y. Cao, Prof. D. Jena
Department of Electrical Engineering
University of Notre Dame
Notre Dame, Indiana 46556 (USA)

DOI: 10.1002/adfm.200800984

structures for high-electron-mobility transistors (HEMTs)[20] and near-infrared intersubband (ISB) devices.[21] As the performance of these devices often degrade at elevated temperature, knowledge of the thermal conductivity is needed to understand the temperature distributions within high power devices and devise approaches for effective thermal management.[22] Our findings offer guidelines for efficient thermal engineering of GaN-based electronic and optical devices, specifically those that use superlattices as either nucleation or active layers.

2. Experimental

We grow AlN–GaN superlattices by nitrogen-source radio-frequency MBE (RFMBE) on top of semi-insulating 3.6 μm GaN templates (prepared by MOCVD) on sapphire substrates. Details of the growth conditions are given in Ref. [18]. All growths are performed under metal rich conditions at 800 °C. As the misfit strain of epitaxial AlN on GaN is relatively high (2.4%), we keep the thickness of the AlN layer (≈4 nm) within the pseudomorphic growth limit to maintain smoothness and to avoid cracks [18].

We grew two sets of superlattices. Set A consists of $(AlN)_{4.1\,nm}$–$(GaN)_{55\,nm}$ superlattices grown under different conditions: the rf power input to the nitrogen plasma was varied from 150 to 400 W, Al flux from 0.4 to 1.7×10^{-7} Torr, and Ga flux from 1.0 to 2.4×10^{-7} Torr. Set B consists of superlattices with different structure $(AlN_x–GaN_y)_n–AlN_x$, where $x \approx 4$ nm, $2\,nm < y < 100$ nm, and $5 < n < 30$, n is the number of periods, grown under the condition that gives the lowest Λ (plasma power of 275 W, an Al flux with an equivalent pressure of 1.5×10^{-7} and a Ga flux with an equivalent pressure of 1.4×10^{-7} Torr). Total thicknesses of the superlattices range from 200 to 500 nm. To extend our studies to structures with thick GaN layer, we grew tri-layer structures of $AlN_x–GaN_y–AlN_x$, where $x \approx 4$ and $200\,nm < y < 1000$ nm. We characterized the thickness of the AlN and GaN layers in the superlattices by comparing simulations and measurements of X-ray diffraction spectra, see Figure 1.

We measure the thermal conductivity Λ by time-domain thermoreflectance [23,24]. Details of our setup are described in Ref. [3]. In this study, the modulation frequency of the pump beam is fixed at 10 MHz. The radii of the pump and probe beam are 15 μm at the sample surface. We use total laser powers of ~30 mW, creating temperature rises of < 5 K. To prepare the samples for measurements, samples are coated with ≈100 nm thick Al films by magnetron sputter deposition. We analyze the data following procedures described in Ref. [25], taking into account changing of the radius of the pump beam at different relative delay time between the pump and probe pulses [26]. In the analyses, we represent our samples as a layer of n-period superlattices ($n = 1$ for the tri-layer structures) and a bottom layer of ~4 nm AlN with $\Lambda = 7\ W\ m^{-1}\ K^{-1}$; this choice does not significantly alter the value of derived Λ compared to the usual approach of modeling the superlattices as one layer, and provides a common procedure for comparing data for the superlattices and for the tri-layer structures.

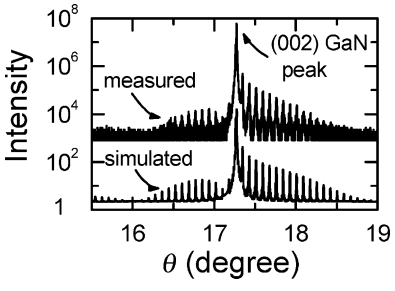

Figure 1. XRD measurement and simulation of an $(AlN)_{4.1\,nm}$–$(GaN)_{52\,nm}$ superlattice. θ is the Bragg angle. The thicknesses of AlN and GaN layers are determined by fitting the simulations to the data.

3. Results and Discussion

We summarize the effect of growth conditions on the Λ of superlattices in Figure 2. All superlattices in Figure 2 have similar structures—$8 \times (4.1 \pm 0.6$ nm AlN/55 ± 3 nm GaN). Nevertheless, the thermal and electrical properties—cross-plane thermal conductivity Λ at room temperature, in-plane Hall concentration $n_{2\text{-}D}$ at 77 K, and in-plane Hall mobility μ at 77 K—vary significantly (see Fig. 2). Unfortunately, we could not determine the cause of these variations because of the complicated carrier distributions in the superlattices. Spatially separated electrons (2DEG) and holes (2DHG) are induced[27] in the superlattices due to polarization-induced band-bending, and the carrier concentration at each AlN/GaN heterojunction depends on the local strain[28] and may not be homogenous. As a result, $n_{2\text{-}D}$, derived from μ and the electrical conductivity may deviate significantly from the total carrier concentration. Moreover, μ is a weighted average of the mobilities of 2DEGs and 2DHGs and is most sensitive to carriers with high mobility. As the mobility of 2DEGs and 2DHGs at low temperature depends on both the carrier density and the interface roughness,[29] mobility of 2DEG and 2DHG may vary for different AlN/GaN heterojunctions. Hence, μ could be strongly affected by atypical properties of certain heterojunctions. Fortunately, Λ is relatively insensitive to carrier concentration. An inhomogeneous distribution of strain could, in principle, contribute to phonon scattering at the interfaces but since the thin AlN layers are planar and have the same in-plane lattice parameter as GaN, the strain field is

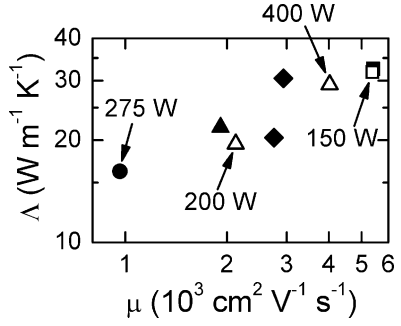

Figure 2. Room temperature thermal conductivity of $(AlN)_{4.1\,nm}$–$(GaN)_{55\,nm}$ superlattices of set A, plotted as a function of the in-plane Hall mobility μ measured at 77 K. The in-plane Hall carrier concentrations at 77 K are $n_{2\text{-}D} =$ 0.9 (circles), 3 (diamonds), 7 (triangles), and 9 (squares) $\times 10^{13}\ cm^{-2}$; electrons are the dominant carriers. Solid symbols are superlattices grown at plasma power $P = 275$ W and open symbols are superlattices grown at the plasma power as labeled. For $P = 275$ W, different Al and Ga fluxes were used to modify $n_{2\text{-}D}$ and μ of the superlattices.

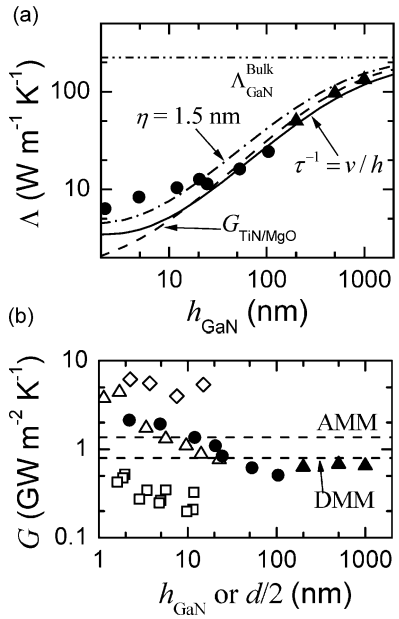

Figure 3. a) Thermal conductivity of $(AlN)_x$–$(GaN)_y$ superlattices (solid circles) and tri-layer structures (solid triangles) of set B plotted as a function of the thickness of the individual GaN layer; the thermal conductivity of bulk GaN [32] is included for comparison. All samples are grown with a plasma power of 275 W, an Al flux with an equivalent pressure of 1.5×10^{-7} Torr, and a Ga flux with an equivalent pressure of 1.4×10^{-7} Torr. The thickness of the AlN layer in all samples is ≈4 nm. The solid line is a calculation using a Debye–Callaway model with the assumption of a boundary scattering length that is equal to the thickness of the individual GaN layers. Minimum thermal conductivities[4] of AlN and GaN are added to the calculation to account for heat transport by high frequency acoustic and optical phonons. The dashed line is the effective thermal conductivity calculated by assuming that each AlN/GaN interface has a thermal conductance equal to the conductance of TiN/MgO interfaces.[33] The dash-dotted line is the sum of the minimum thermal conductivity and a calculation of the thermal conductivity using a Debye–Callaway model with the assumption that the boundary scattering rate varies with phonon wavelength; the fitting parameter is $\eta = 1.5$ nm, see Eq. 3. b) The mean thermal conductance of interfaces in the superlattices (solid circles) and tri-layers (solid triangles) of set B derived from the thermal conductivity measurements shown in (a). The mean thermal conductance of interfaces in GaAs/AlAs [34] superlattices (open triangles), $Si/Si_{0.7}Ge_{0.3}$ [35] superlattices (open diamonds) and W/Al_2O_3 [5] multilayers (open squares) are included for comparison and are plotted as a function of half of the period, $d/2$. The dashed lines are the mean thermal conductance of AlN/GaN interfaces calculated using the AMM and DMM.

homogeneous and confined to the AlN layer. We do not expect this homogeneous strain field in the AlN layers to significantly alter the phonon lifetimes. Hence, we tentatively attribute the variation in the Λ to interface roughness. This is in keeping with the trend in the low-temperature mobility; Λ increases as the low-temperature μ increases, probably due to reduced interface roughness scattering.

We measure the Λ of AlN_x–GaN_y superlattices over a wide range of GaN thickness, see Figure 3a. All of the data plotted in Figure 3 are for samples grown under the condition that gives the lowest Λ in Figure 2. We find that Λ decreases monotonically as the thickness of the GaN layer decreases, reaching $\Lambda = 6.35\ \mathrm{W\ m^{-1}\ K^{-1}}$ at $y = 2.2$ nm, comparable to the thermal conductivity of alloy $Al_{0.44}Ga_{0.56}N$ thin film[30] of $5.55\ \mathrm{W\ m^{-1}\ K^{-1}}$.

To gain insights into the data, we evaluate our data using two complementary approaches. In the first approach, we attribute the additional thermal resistance in the superlattices to the thermal resistance of the interfaces. We assume that the thermal resistance of individual layers and interfaces add in series, and estimate the harmonic mean of the thermal conductance G of interfaces from our Λ measurements using

$$\frac{2}{G} = \frac{x+y}{\Lambda} - \frac{x}{\Lambda_{\mathrm{AlN}}^{\mathrm{Bulk}}} - \frac{y}{\Lambda_{\mathrm{GaN}}^{\mathrm{Bulk}}} \quad (1)$$

where $\Lambda_{\mathrm{AlN}}^{\mathrm{Bulk}}$ and $\Lambda_{\mathrm{GaN}}^{\mathrm{Bulk}}$ are thermal conductivities of bulk AlN[31] and GaN,[32] respectively. The derived values of G using this approach are plotted in Figure 3b. For $y > 40$ nm, $G \approx 620\ \mathrm{W\ m^{-2}\ K^{-1}}$, close to the thermal conductance of epitaxial interfaces between two similar materials with high speeds of sound (e.g., TiN/MgO[33]). For $y < 40$ nm, G increases with decreasing GaN thickness; possible reasons for this increase are discussed below. This increase of apparent thermal conductance is not unique to AlN/GaN superlattices; similar trends are observed in short-period superlattices and multilayers of GaAs/AlAs,[34] $Si/Si_{0.7}Ge_{0.3}$,[35] and W/Al_2O_3,[5] see Figure 3b.

In the second approach, we disregard the thermal resistance of the interfaces and instead consider the scattering of phonons at interfaces. Hence, we add an additional boundary scattering rate $\tau^{-1} = v/h$, where h is the thickness of superlattice layers and v is the speed of sound. We construct a Debye-Callaway model following the work of Morelli et al.[36] and include this additional scattering term in the model. Details of our approach are described in Ref. [26]; the parameters of the model are summarized as Table 1. We approximate the cutoff frequencies from the peaks of the calculated phonon density of states.[37] We fix the relative anharmonic scattering strengths of umklapp and normal processes, B_U and B_N, and obtain absolute values of the anharmonic scattering strengths from fits to the thermal conductivity of bulk AlN[31] and GaN,[32] see Figure 5. We calculate the strengths of Rayleigh scattering Γ due to isotopes of nitrogen and gallium from Eq. (16) of Ref. [36]; $\Gamma = 4.29 \times 10^{-6}$ for AlN and $\Gamma = 2.74 \times 10^{-4}$ for GaN. We then estimate the Λ of superlattices from

$$\frac{x+y}{\Lambda} = \frac{x}{\Lambda_{\mathrm{AlN}}^{\mathrm{Cal}}} + \frac{y}{\Lambda_{\mathrm{GaN}}^{\mathrm{Cal}}} \quad (2)$$

where $\Lambda_{\mathrm{AlN}}^{\mathrm{Cal}}$ and $\Lambda_{\mathrm{GaN}}^{\mathrm{Cal}}$ are thermal conductivities of AlN and GaN layers calculated from this Debye-Callaway model.

Our Debye-Callaway model does not include heat transport by optical phonons and, because of the relatively low cut-off frequencies for the acoustic branches, greatly restricts the number of acoustic phonons that are included in the modeling; in fact, <10% of the 3N vibrational modes of the crystal are included in this approach. To account for heat transport by phonons that are neglected by the model, we estimate the thermal conductivity of these phonons using the calculated minimum thermal conductivities[4] of AlN and GaN.

Table 1. Speeds of sound (ν), cutoff frequencies (θ), strengths of Rayleigh scattering (Γ), and anharmonic scattering (B) for GaN and AlN used in the Debye-Callaway model. The definitions of Γ and B are given in Ref. [36]. The subscripts L and T represent longitudinal and transverse phonons, respectively. The superscripts U and N represent umklapp and normal three-phonon processes, respectively.

	ν_L [m s^{-1}]	ν_T [m s^{-1}]	θ_L [K]	θ_T [K]	Γ	B_L^U [10^{-19} s K^{-1}]	B_T^U [10^{-19} s K^{-1}]	B_L^N [10^{-19} s K^{-1}]	B_T^N [10^{-19} s K^{-1}]
GaN	8080	4150	441	213	2.74×10^{-4}	0.32	1.23	0.51	1.86
AlN	10930	6200	754	352	4.29×10^{-6}	0.42	1.37	0.83	2.23

The calculations of the Debye–Callaway model added to the minimum thermal conductivity are plotted as a solid line in Figure 3a; the effective thermal conductivity estimated from the first approach calculated using the thermal conductance of TiN/MgO interfaces[33] is plotted as a dashed line. Both calculations agree well with the data for $y > 40$ nm, but deviate from the data for $y < 40$ nm.

One possible explanation of the discrepancies between these models and the data for short-period superlattices is that the interface morphology depends on the GaN layer thickness y; e.g., the roughness of interfaces might be small at small values of y and large at $y > 40$ nm. Since phonons are diffusely scattered at rough interfaces but coherently transmitted and reflected at smooth interfaces, G could be larger for smoother interfaces.[6] However, we do not expect the difference in G to be as large as a factor of 3.5 for interfaces between two similar materials. We note that the thermal conductance estimated from a model assuming that phonons are diffusely scattered [diffuse mismatch model (DMM)][6] and from another model assuming phonons are coherently transmitted and reflected [acoustic mismatch model (AMM)][38] at the interface are 0.8 and 1.4 GW m^{-2} K^{-1}, respectively, see Figure 3b. In the calculations of the DMM and AMM models, we consider only acoustic modes by treating each AlN and GaN molecule as a single unit. We assume a linear, Debye-like dispersion for these acoustic modes, and treat the longitudinal and transverse modes separately. We allow mode conversions[6,38] in the calculations.

A second possibility is that the excess heat is carried by optical phonons which are not accounted for in the Debye-Callaway model. Even though the group velocity of optical phonons is typically small, high energy optical modes may still contribute a significant portion of heat conduction in short-period superlattices through tunneling[7] and mode conversion,[8] as most acoustic modes are scattered by the interfaces. To test this idea, we bombarded a GaN template and an $(AlN)_{4.1\ nm}$–$(GaN)_{4.9\,nm}$ superlattice with 2.3 MeV Ar^+ ions of different doses to create point defects in the GaN template and the superlattice.

In the analysis of TDTR data of the ion-bombarded GaN, we subdivide the GaN template into five layers according to the simulated damage profile and assume that Λ is uniform within each layer; Λ derived from this approach differs by less than 25% from Λ derived from the usual procedure of assuming the GaN template as a single layer. The derived Λ of the ion-bombarded GaN is reduced by an order of magnitude for ion dose of 2.6×10^{14} ions cm^{-2}. The reduction in Λ of the ion-bombarded superlattice, however, is $<35\%$, see Figure 4.

We assume that ion bombardments create mainly point defects such as vacancies and substitutional atoms, and interstitials; hence, we expect that the strength of Rayleigh scattering Γ created by the ion bombardment will be proportional to ion dose. We include phonon scattering by these point defects in the Debye-Callaway model using a Rayleigh scattering term that is proportional to the ion dose; the constant of proportionality is adjusted to fit the data for GaN, see the solid line in Figure 4. From the fit, $\Gamma = 1.0$ for an ion dose of 3×10^{14} ions cm^{-2}. The thermal conductivity of the short period superlattice is reduced by $<35\%$ at high ion dose, see Figure 4. As optical phonons and high frequency acoustic phonons are strongly scattered by point defects,[17] this small reduction of Λ created indicates that optical phonons and high frequency acoustic phonons are not the dominant heat carriers in short-period superlattices.

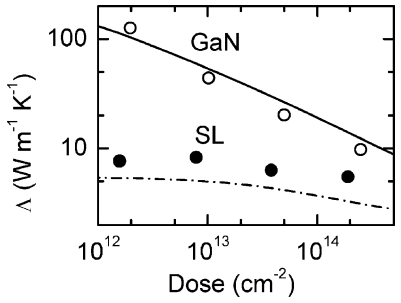

Figure 4. Thermal conductivity of a MOCVD-grown GaN and an $(AlN)_{4.1\ nm}$–$(GaN)_{4.9\,nm}$ superlattice bombarded by 2.3 MeV Ar^+ ions plotted as a function of ion dose. The solid line is the sum of the minimum thermal conductivity and a calculation of the thermal conductivity using a Debye-Callaway model with the assumption of a Rayleigh scattering strength that is proportional to ion dose; the constant of proportionality is adjusted to fit the data. The dash-dotted line is the sum of the minimum thermal conductivity and a calculation of the thermal conductivity using a Debye-Callaway model with the assumptions i) that the boundary scattering rate varies with phonon wavelength ($\eta = 1.5$ nm, $h_{AlN} = 4$ nm, and $h_{GaN} = 5$ nm), see Eq. 3; and ii) the Rayleigh scattering strength has the same linear dependence on ion dose as in GaN.

A third possibility is the formation of phonon minibands due to the interference of phonons that are coherently reflected from multiple interfaces. Since more phonons are transmitted in phonon minibands compared to interfaces acting independently,[16] the formation of phonon minibands enhances the apparent thermal conductance G and therefore enhances the Λ.[10] This is akin to enhancement of electronic conductivity by the formation of electron minibands in superlattices. To test this idea, we measured the temperature dependence of the thermal conductivity Λ of a short-period superlattice ($y = 4.9$ nm) and two superlattices ($y \approx 55$ nm) grown under different conditions; Λ decreases with decreasing temperature for all three superlattices, see Figure 5. This behavior is expected if scattering of phonons is dominated by boundary or interface scattering, but is inconsistent with a description based on the formation of phonon minibands.

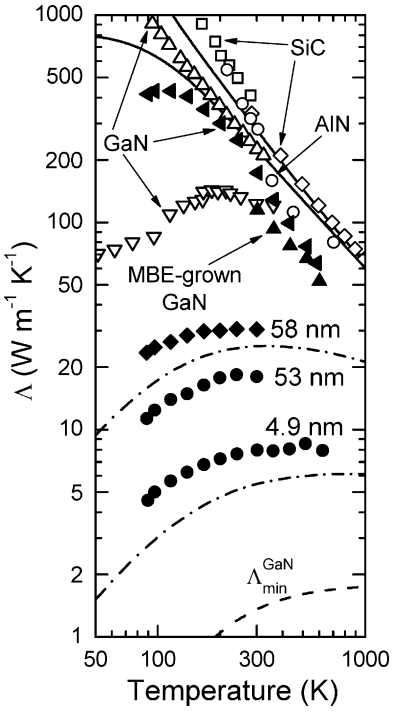

Figure 5. Temperature dependence of thermal conductivity of MOCVD-grown 3.6 μm GaN (left solid triangles), MBE-grown 0.69 μm GaN (up solid triangles), and superlattices grown under the condition that gives the highest (solid diamonds) and the lowest (solid circles) thermal conductivities. Data for the thermal conductivity of AlN from Ref. [31] (open circles); GaN from Ref. [32] (up open triangles) and Ref. [40] (down open triangles); and SiC from Ref. [41] (open squares) and Ref. [42] (open diamonds) are included for comparison. The superlattices are labeled by the thickness of the individual GaN layers. The solid lines are calculations using a Debye-Callaway model with the strength of the anharmonic phonon scattering rates adjusted to fit the thermal conductivity of pure AlN [31] and GaN. [32] The dashed line is the minimum thermal conductivity [4] of GaN. The upper and lower dash-dotted lines are the sum of the minimum thermal conductivity and the thermal conductivity calculated using a Debye-Callaway model with the assumption that the boundary scattering rate varies with phonon wavelength ($\eta = 1.5$ nm, $h_{AlN} = 4$ nm, and $h_{GaN} = 50$ and 5 nm, respectively), see Eq. 3.

If minibands are formed, phonons are not scattered by the interfaces, but are mainly scattered by the umklapp process with a modified dispersion.[9] Thus, the temperature dependence suggests that only a small fraction of phonons that are able to average over the interface roughness are able to form minibands.

A fourth possibility is that transmission of phonons across superlattices might be a strong function of phonon wavelength; e.g., interfaces are more efficient at scattering short-wavelength phonons and the transmission coefficient of long-wavelength phonons is relatively high.[39] Thus, for small y, where the thermal conductivity is small, long-wavelength phonons provide a larger fraction of the heat transport and the apparent G is high. We incorporate this idea into the Debye-Callaway model using a boundary scattering rate that depends on phonon wavelength. We define a boundary scattering length $\ell = h/(1-p)$, where $p = \exp(-\eta^2/\lambda^2)$ is the fraction of incident phonons that are specularly scattered at the interfaces,[39] η is a fitting parameter that depends on interface roughness, and λ is the wavelength of the phonon. The parameter η has units of length, and while we expect that η is on the same order as the rms roughness of the interfaces, other factors – e.g., the acoustic impedance mismatch and the in-plane correlation length of the roughness – will also contribute to the value of η. The scattering rate is then

$$\tau^{-1} = \frac{v}{h}\left(1 - \exp\left(-\frac{\eta^2}{\lambda^2}\right)\right) \quad (3)$$

where v is the speed of sound. Calculations using the Debye-Callaway model including the minimum thermal conductivity in combination with Equation 3 are plotted as dash-dotted lines in Figures 3a, 4 and 5. The calculations fit well with the period, temperature and ion-dose dependence of Λ.

4. Conclusions

In conclusion, we report the thermal conductivity Λ of AlN–GaN superlattices over a wide range of layer thicknesses, $2 < h < 1000$ nm, temperature $90\ \mathrm{K} < T < 600\ \mathrm{K}$, and point defect density created by ion bombardment. A single model for the phonon scattering rates successfully fits all of the data. We conclude from our experiments and modeling that long-wavelength phonons are the dominant carriers of heat in AlN–GaN short period superlattices and that the scattering of long-wavelength phonons at AlN/GaN interfaces has a strong dependence on phonon wavelength.

Acknowledgements

This work was supported by ONR grant no. N00014-07-1-0190. Sample characterization used the facilities of the Center of Microanalysis of Materials which is partially supported by the US Department of Energy under grant no. DEFG02-91ER45439; and Laser Facility of the Frederick Seitz Materials Research Laboratory (MRL) at UIUC. One of the authors (Debdeep Jena) thanks Dr. Mark Rosker (DARPA) for useful discussions.

Received: July 15, 2008
Revised: November 3, 2008
Published online:

[1] R. Venkatasubramanian, E. Siivola, T. Colpitts, B. O'Quinn, *Nature* **2001**, *413*, 597.
[2] T. C. Harman, P. J. Taylor, M. P. Walsh, B. E. LaForge, *Science* **2002**, *297*, 2229.
[3] D. G. Cahill, W. K. Ford, K. E. Goodson, G. D. Mahan, A. Majumdar, H. J. Maris, R. Merlin, S. R. Phillpot, *J. Appl. Phys.* **2003**, *93*, 793.
[4] D. G. Cahill, R. O. Pohl, *Annu. Rev. Phys. Chem.* **1988**, *39*, 93.
[5] R. M. Costescu, D. G. Cahill, F. H. Fabreguette, Z. A. Sechrist, S. M. George, *Science* **2004**, *303*, 989.
[6] E. T. Swartz, R. O. Pohl, *Rev. Mod. Phys.* **1989**, *61*, 605.
[7] B. K. Ridley, *Phys. Rev. B* **1994**, *49*, 17253.
[8] A. A. Kiselev, K. W. Kim, M. A. Stroscio, *Phys. Rev. B* **2000**, *62*, 6896.

[9] S. Y. Ren, J. D. Dow, *Phys. Rev. B* **1982**, *25*, 3750.
[10] M. V. Simkin, G. D. Mahan, *Phys. Rev. Lett.* **2000**, *84*, 927.
[11] R. Venkatasubramanian, *Phys. Rev. B* **2000**, *61*, 3091.
[12] S. Chakraborty, C. A. Kleint, A. Heinrich, C. M. Schneider, J. Schumann, M. Falke, S. Teichert, *Appl. Phys. Lett.* **2003**, *83*, 4184.
[13] S.-M. Lee, D. G. Cahill, R. Venkatasubramanian, *Appl. Phys. Lett.* **1997**, *70*, 2957.
[14] M. N. Touzelbaev, P. Zhou, R. Venkatasubramanian, K. E. Goodson, *J. Appl. Phys.* **2001**, *90*, 763.
[15] B. Yang, G. Chen, *Phys. Rev. B* **2003**, *67*, 195311.
[16] Y. Chen, D. Li, J. R. Lukes, Z. Ni, M. Chen, *Phys. Rev. B* **2005**, *72*, 174302.
[17] P. G. Klemens, *Proc. R. Soc. Lond.* **1955**, *A68*, 1113.
[18] Y. Cao, D. Jena, *Appl. Phys. Lett.* **2007**, *90*, 182112.
[19] E. Sarigiannidou, E. Monroy, N. Gogneau, G. Radtke, P. Bayle-Guillemaud, E. Bellet-Amalric, B. Daudin, J. L. Rouvière, *Semicond. Sci. Technol.* **2006**, *21*, 612.
[20] M. Higashiwaki, T. Mimura, T. Matsui, *IEEE Electron Device Lett.* **2006**, *27*, 719.
[21] F. R. Giorgetta, E. Baumann, F. Guillot, E. Monroy, D. Hofstetter, *Eletron. Lett.* **2007**, *43*, 185.
[22] J. Xu, W.-Y. Yin, J. Mao, *IEEE Microw. Wirel. Compon. Lett.* **2007**, *17*, 55.
[23] C. A. Paddock, G. L. Eesley, *J. Appl. Phys.* **1986**, *60*, 285.
[24] D. A. Young, C. Thomsen, H. T. Grahn, H. J. Maris, J. Tauc, in *Phonon Scattering in Condensed Matter*, (Eds: A. C. Anderson, J. P. Wolfe), Springer, Berlin, Germany **1986**, p. 49.
[25] D. G. Cahill, *Rev. Sci. Instrum.* **2004**, *75*, 5119.
[26] Y. K. Koh, D. G. Cahill, *Phys. Rev. B* **2007**, *76*, 075207.
[27] S. Acar, S. B. Lisesivdin, M. Kasap, S. Özçelik, E. Özbay, *Thin Solid Films* **2008**, *516*, 2041.
[28] O. Ambacher, J. Smart, J. R. Shealy, N. G. Weimann, K. Chu, M. Murphy, W. J. Schaff, L. F. Eastman, R. Dimitrov, L. Wittmer, M. Stutzmann, W. Rieger, J. Hilsenbeck, *J. Appl. Phys.* **1999**, *85*, 3222.
[29] D. K. Ferry, S. M. Goodnick, *Transport in Nanostructures*, Cambridge University Press, Cambridge, United Kingdom **1999**, p. 453.
[30] B. C. Daly, H. J. Maris, A. V. Nurmikko, M. Kuball, J. Han, *J. Appl. Phys.* **2002**, *92*, 3820.
[31] G. A. Slack, R. A. Tanzilli, R. O. Pohl, J. W. Vandersande, *J. Phys. Chem. Solids* **1987**, *48*, 641.
[32] G. A. Slack, L. J. Schowalter, D. Morelli, J. A. Freitas, Jr, *J. Cryst. Growth* **2002**, *246*, 287.
[33] R. M. Costescu, M. A. Wall, D. G. Cahill, *Phys. Rev. B* **2003**, *67*, 054302.
[34] W. S. Capinski, H. J. Maris, T. Ruf, M. Cardona, K. Ploog, D. S. Katzer, *Phys. Rev. B* **1999**, *59*, 8105.
[35] S. T. Huxtable, A. R. Abramson, C.-L. Tien, A. Majumdar, C. LaBounty, X. Fan, G. Zeng, J. E. Bowers, A. Shakouri, E. T. Croke, *Appl. Phys. Lett.* **2002**, *80*, 1737.
[36] D. T. Morelli, J. P. Heremans, G. A. Slack, *Phys. Rev. B* **2002**, *66*, 195304.
[37] H. M. Tütüncü, G. P. Srivastava, S. Duman, *Physica B* **2002**, *316-317*, 190.
[38] W. A. Little, *Can. J. Phys.* **1959**, *37*, 334.
[39] J. M. Ziman, *Electrons and Phonons*, Clarendon, Oxford, United Kingdom **1960**, p. 456.
[40] E. K. Sichel, J. I. Pankove, *J. Phys. Chem. Solids* **1977**, *38*, 330.
[41] D. Morelli, J. Hermans, C. Beetz, W. S. Woo, G. L. Harris, C. Taylor, in *Silicon Carbide and Related Materials*, N137 M. G. Spencer, R. P. Devaty, J. A. Edmond, M. Asif Khan, R. Kaplan, M. Rahman), IOP Publishing, Bristol, United Kingdom **1993**, p. 313.
[42] O Nilsson,, H. Mehling, R. Horn, J. Fricke, R. Hofmann, S. G. Müller, R. Eckstein, D. Hofmann, *High Temp.-High Pressures* **1997**, *29*, 73.